Topology-cognizant Optimal Power Flow in Multi-terminal DC Grids

Tuncay Altun, *Student Member, IEEE,* Ramtin Madani, *Member, IEEE,* and Ali Davoudi, *Senior Member, IEEE*

***Abstract*—This paper is concerned with the optimization of droop control set-points, i.e., voltage and power levels at each bus, and the switching status of transmission lines, in multi-terminal direct current grids. Additional constraints, that ensure a safe operation in response to power fluctuation while updating droop set-points, are integrated into the problem formulation. This problem is cast as a mixed-integer nonlinear program with three sources of computational complexity: i) Non-convex power flow equations, (ii) Non-convex converter loss equations, and iii) Binary variables accounting for the on/off status of transmission lines. Second-order cone programming relaxation tackles the non-convexity of power flows and converter loss equations, and branch-and-bound search determines the optimal switching status of transmission lines. CIGRE B4 DC grid benchmark is emulated in a real-time hardware-in-the-loop environment to corroborate the proposed method.**

***Index Terms*—HVDC transmission, multi-terminal dc grids, optimal power flow, optimal transmission switching.**

I. Introduction

Multi-terminal direct current (MTDC) grids are becoming popular as they allow efficient power exchange between synchronized or unsynchronized power grids, and are suitable candidates for integrating offshore wind farms [1] or long-distance power transmission (e.g., European supergrid [2]) as its DC grid enjoys a simpler control mechanism and avoids challenges native to AC grids. Voltage-source converters (VSCs) are building blocks of MTDC grids and allow interconnection with weak AC grids [3], black start in the case of blackouts, [4] and power flow reversal without switching the voltage polarity [5]. There are ongoing efforts to realize bulk power exchange among independent grids using the VSC technology [6]. Control of the VSC's DC voltage is the key measure to proper power dispatch and loss management in a MTDC grid, and is mainly done via master-slave [7], voltage margin [8], or voltage droop [9] mechanisms. Voltage margin control can cause an oscillatory behavior [10]. Droop control approach is more reliable than the master-slave control if several converters actively participate in the regulation process.

The two-tier control hierarchy of MTDC grids [11], [12] includes a faster, lower-level droop controller that locally regulates the VSC voltage at the cost of power sharing objectives. Hence, the upper-level optimizer periodically tunes the set-points of the lower-level droop control to meet predefined objectives, i.e, minimizing generation cost, transmission loss, etc. The optimization involved in tuning droop set-points could become computationally prohibitive for real-time applications [13]. This delay, or any interruption in the communication between the two control layers, could cause a prescribed droop set-point to violate an operational safety limit, particularly if the load demand or power generation fluctuate noticeably before the subsequent droop set-points update [14]–[16]. Preventive measures, while still pursuing optimality in MTDC grids, are rare in the literature, e.g., see [17]–[19].

The optimal power flow (OPF) in MTDC grids aims to minimize transmission loss alone [11] or along with conversion loss [20]. Convex relaxation methods, including semi-definite programming (SDP) and second-order cone programming (SOCP), can transform nonlinear power flow optimization into convex surrogates by reformulating it in a high-dimensional space while preserving equivalency with the original non-convex problem [21]. The SDP and SOCP relaxations, and their variations, have manifested notable success in solving OPF problems in AC systems [22], [23]. These approaches have been extended to the static OPF problem of MTDC grids that suffer from additional non-convexity due to the presence of quadratic converter loss equations [24], [25].

Static OPF solutions, however, overlook the optimal switching of transmission lines that can help alleviate line overloads, address voltage violations, minimize transmission losses, protect the grid from abnormal operations, or schedule maintenance [26]. In fact, a transmission line built for a long-term requirement could exhibit dispatch inefficiencies [27]. Recently, mixed-integer cone programming techniques have been used to solve AC grid topology problems [28], [29]. In this paper, we offer a mixed-integer second-order cone programming (MISOCP) formulation for the topology-cognizant OPF in MTDC grids to minimize both transmission and converter losses. The proposed formulation includes safety constraints that prevent voltage violations caused by power fluctuation in between two droop set-point updates. In summary, the salient contributions of this paper are listed as follows:

- The static OPF problem of MTDC grids, with the objective of minimizing the total loss, is formulated as a nonlinear optimization while respecting pyhsical and operational constraints for both AC and DC parts.
- Additional constraints that sustain a safe operation by further restricting voltage limits, in response to volatile generation/load profiles in between two droop set-point updates, are integrated into the problem formulation.
- Static OPF formulation is extended to a topology-cognizant OPF by incorporating binary variables that represent the switching status of transmission lines.

This work is supported by the National Science Foundation under award ECCS-1809454. The authors are with the University of Texas at Arlington, TX, 76019, USA (e-mail: tuncay.altun@mavs.uta.edu; ramtin.madani@uta.edu; davoudi@uta.edu).

- The proposed MISOCP surrogate is formulated for topology-cognizant OPF problem.
- The proposed static OPF, topology-cognizant OPF without safety constraints, and topology-cognizant OPF with safety constraints are experimentally validated through real-time hardware-in-the-loop (HIL) experiments.

The remainder of the paper is organized as follows. Section II covers preliminary materials. Section III elaborates the modeling of MTDC grids. Section IV integrates the switching statuses of transmission lines into the OPF problem, and provides its MISOCP-relaxed formulation. In Section V, the resulting SOCP-relaxed OPF and MISOCP-relaxed topology-cognizant OPF problems are verified for the CIGRE B4 DC grid benchmark using a real-time HIL. Section VII concludes the paper.

II. Notations and Grid Terminologies

A. Notations

Bold uppercase and lowercase letters (e.g., $\boldsymbol{X}$, $\boldsymbol{x}$) represent matrices and vectors, respectively. $\mathbf{1}$ and $\mathbf{0}$ refer to vectors with all elements as 1 and 0, respectively. The $\mathbb{R}$ and $\mathbb{C}$ symbolize the sets of real and complex numbers, respectively. $\mathbb{S}^n$ and $\mathbb{H}^n$ represent the $n \times n$ symmetric and hermitian matrices, respectively. The real and imaginary parts of a complex number or matrix are defined by $\mathrm{real}\{\cdot\}$ and $\mathrm{imag}\{\cdot\}$, respectively. The matrix entries are denoted by indices (i, j). Superscripts $(\cdot)^\top$ and $(\cdot)^*$ denote the transpose and conjugate transpose operator, respectively. $|\cdot|$ represents the cardinality of a set or the absolute/magnitude value of a vector/scalar. $[\cdot]$ creates a matrix whose diagonal elements are obtained from a given vector. $\mathrm{tr}\{\cdot\}$ refers to the trace of a given matrix. $\|\cdot\|_2$ stands for the euclidean norm of a given vector. $\mathrm{diag}\{\cdot\}$ composes a vertical vector from the diagonal elements of a given matrix. $\boldsymbol{X} \succeq 0$ means that $\boldsymbol{X}$ is a symmetric positive semidefinite matrix.

B. Grid Terminologies

Figure 1 shows a portion of an MTDC grid. Grid buses are connected via DC transmission lines. Terminologies for grid elements are elaborated here:

- **DC Grid:** The DC transmission grid can be structured as a directed graph $\mathcal{H} = (\mathcal{N}, \mathcal{L})$, with $\mathcal{N}$ and $\mathcal{L}$ as the sets of buses and lines, respectively. Define the pairs $\vec{\boldsymbol{L}}, \overleftarrow{\boldsymbol{L}} \in \{0,1\}^{|\mathcal{L}|\times|\mathcal{N}|}$ as the *from* and *to* line-incidence matrices for the DC grid, respectively. For every $l \in \mathcal{L}$ and $k \in \mathcal{N}$, $\vec{L}_{lk} = 1$ if and only if the transmission line l starts at bus k, and $\overleftarrow{L}_{lk} = 1$ if and only if the line l ends at bus k. The matrices $\boldsymbol{Y} \in \mathbb{R}^{|\mathcal{N}|\times|\mathcal{N}|}$, $\vec{\boldsymbol{Y}}, \overleftarrow{\boldsymbol{Y}} \in \mathbb{R}^{|\mathcal{L}|\times|\mathcal{N}|}$ represent the bus-conductance, and the *from* and *to* line-conductance matrices of the DC grid, respectively. Define $\vec{\boldsymbol{f}}$ and $\overleftarrow{\boldsymbol{f}} \in \mathbb{R}^{|\mathcal{L}|}$ as the *from* and *to* vectors of transmission line power flows, respectively. Let $\vec{\boldsymbol{f}}^{\max} \in (\mathbb{R} \cup \{\infty\})^{|\mathcal{L}|}$ be the vector of power flow limits. Additionally, define $\vec{\boldsymbol{x}} \in \{0,1\}^{|\mathcal{L}|}$ as the binary vector representing the on/off switching status of transmission lines. Let $\vec{\boldsymbol{x}}_{\min}, \vec{\boldsymbol{x}}_{\max} \in \{0,1\}^{|\mathcal{L}|}$ encapsulate prior knowledge of the on/off switches, i.e.,

$$\vec{x}_{\min_l} = \vec{x}_{\max_l} = 0, \quad \text{if line } l \in \mathcal{L} \text{ is known to be disconnected,}$$

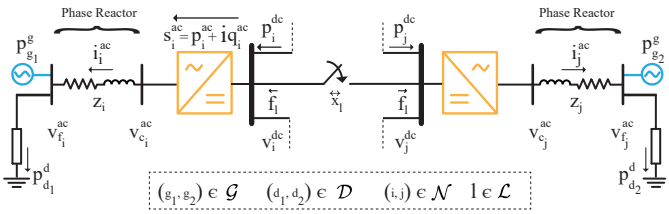

Fig. 1. A portion of a meshed MTDC grid. The grid is endowed with switching devices to enable line switching decisions, $\vec{\boldsymbol{x}}$. VSCs couple AC and DC parts by controlling their voltage and power levels on both sides.

$$\vec{x}_{\min_l} = \vec{x}_{\max_l} = 1, \quad \text{if line } l \in \mathcal{L} \text{ is known to be connected,}$$
$$\vec{x}_{\min_l} = 0, \quad \vec{x}_{\max_l} = 1, \text{otherwise.}$$

Finally, let $\boldsymbol{v}^{\mathrm{dc}}, \boldsymbol{p}^{\mathrm{dc}} \in \mathbb{R}^{|\mathcal{N}|}$ represent the vectors of nodal DC voltages and active power injections into the DC side.

- **Buses/VSCs:** Each DC bus $k \in \mathcal{N}$ is assumed to accommodate a single voltage-source converter (VSC) which is connected to a set of loads and generators through a phase reactor, modeled as a series impedance $z_k \in \mathbb{C}$. Define $\boldsymbol{z}, \boldsymbol{i}^{\mathrm{ac}} \in \mathbb{C}^{|\mathcal{N}|}$ as the vectors of phase-reactor impedance and current values, respectively. Let $\boldsymbol{v}_{\mathrm{c}}^{\mathrm{ac}}, \boldsymbol{v}_{\mathrm{f}}^{\mathrm{ac}} \in \mathbb{C}^{|\mathcal{N}|}$ account for the vectors of VSC and load/generation-side AC voltages, respectively. Let $\boldsymbol{s}^{\mathrm{ac}} \in \mathbb{C}^{|\mathcal{N}|}$, and $\boldsymbol{p}^{\mathrm{ac}}, \boldsymbol{q}^{\mathrm{ac}} \in \mathbb{R}^{|\mathcal{N}|}$, respectively, represent the vectors of apparent, active and reactive power injections from VSCs into the AC sides.
- **Generators/Loads:** Define $\mathcal{G}$ as the set of generators and $\boldsymbol{G} \in \{0,1\}^{|\mathcal{G}|\times|\mathcal{N}|}$ as the generator incidence matrix, where $G_{gk} = 1$ if and only if the generator $g \in \mathcal{G}$ is located at the AC side of the bus $k \in \mathcal{N}$. $\boldsymbol{s}^{\mathrm{g}} \in \mathbb{C}^{|\mathcal{G}|}$ and $\boldsymbol{p}^{\mathrm{g}}, \boldsymbol{q}^{\mathrm{g}} \in \mathbb{R}^{|\mathcal{G}|}$, respectively, represent the vectors of apparent, active and reactive power generations. Define $\mathcal{D}$ as the set of loads and $\boldsymbol{D} \in \{0,1\}^{|\mathcal{D}|\times|\mathcal{N}|}$ as the load incidence matrix where $D_{dk} = 1$ if and only if the load $d \in \mathcal{D}$ is located at the AC side of the bus $k \in \mathcal{N}$. Finally, $\boldsymbol{p}^{\mathrm{d}} \in \mathbb{R}^{|\mathcal{D}|}$ represents the vectors of active power demand.

III. MTDC Grid Model

A. AC/DC Coupling

VSC losses are approximated by a quadratic polynomial with respect to current magnitude as

$$\boldsymbol{p}_{\mathrm{loss}}^{\mathrm{conv}} \triangleq -\boldsymbol{p}^{\mathrm{ac}} - \boldsymbol{p}^{\mathrm{dc}} = \boldsymbol{a} + [\boldsymbol{b}]|\boldsymbol{i}^{\mathrm{ac}}| + [\boldsymbol{c}]|\boldsymbol{i}^{\mathrm{ac}}|^2, \tag{1}$$

where $\boldsymbol{a}, \boldsymbol{b}, \boldsymbol{c} \in \mathbb{R}^{|\mathcal{N}|}$ are the vectors of positive coefficients [24], and $\boldsymbol{p}^{\mathrm{ac}}$ and $\boldsymbol{p}^{\mathrm{dc}}$ are the vectors of active power injections by the VSCs into the AC and DC sides, respectively. Additionally, the AC and DC side voltages are related with a modulation factor, m,

$$|\boldsymbol{v}_{\mathrm{c}}^{\mathrm{ac}}| \leq \sqrt{\frac{3}{2}} m \boldsymbol{v}^{\mathrm{dc}}. \tag{2}$$

B. VSC Limits

The AC side complex powers can be calculated as

$$\boldsymbol{s}^{\mathrm{ac}} = [\boldsymbol{v}_{\mathrm{c}}^{\mathrm{ac}}] \left([\boldsymbol{z}]^{-1}(\boldsymbol{v}_{\mathrm{c}}^{\mathrm{ac}} - \boldsymbol{v}_{\mathrm{f}}^{\mathrm{ac}})\right)^*, \tag{3}$$

with the VSCs active power is bounded as

$$\boldsymbol{p}^{\mathrm{ac}}_{\min} \le \boldsymbol{p}^{\mathrm{ac}} \le \boldsymbol{p}^{\mathrm{ac}}_{\max}. \tag{4}$$

With no loss of generality, the VSC reactive power limits can be formulated as

$$-m_{\mathrm{b}}|\bar{\boldsymbol{s}}^{\mathrm{ac}}| \le \boldsymbol{q}^{\mathrm{ac}} \le [|\mathrm{imag}\{\boldsymbol{z}\}|]^{-1}\left[\boldsymbol{v}^{\mathrm{ac}}_{\mathrm{c}_{\max}}\right]\left(\boldsymbol{v}^{\mathrm{ac}}_{\mathrm{c}_{\max}} - |\boldsymbol{v}^{\mathrm{ac}}_{\mathrm{f}}|\right), \tag{5}$$

where m_{b} is a positive constant, and $|\bar{\boldsymbol{s}}^{\mathrm{ac}}|$ is the vector of nominal VSC apparent power values [20]. To simplify (5) while finding the maximum reactive power constraint, one can substitute $|\boldsymbol{v}^{\mathrm{ac}}_{\mathrm{f}}|$ with $\boldsymbol{v}^{\mathrm{ac}}_{\mathrm{f}_{\max}}$ [20].

Finally, according to Ohm's law,

$$\boldsymbol{i}^{\mathrm{ac}} = [\boldsymbol{z}]^{-1}(\boldsymbol{v}^{\mathrm{ac}}_{\mathrm{c}} - \boldsymbol{v}^{\mathrm{ac}}_{\mathrm{f}}), \tag{6}$$

and the current magnitude $|\boldsymbol{i}^{\mathrm{ac}}|$, should not exceed an upper limit $|\boldsymbol{i}^{\mathrm{ac}}_{\max}|$, to be compatible with the limits of phase reactor and controller.

C. Generator/Load Limits

Active power balance at the generator/load sides of phase reactors can be formulated as

$$\boldsymbol{G}^{\top}\boldsymbol{p}^{\mathrm{g}} - \boldsymbol{D}^{\top}\boldsymbol{p}^{\mathrm{d}} = \mathrm{real}\left\{[\boldsymbol{v}^{\mathrm{ac}}_{\mathrm{f}}]\left([\boldsymbol{z}]^{-1}(\boldsymbol{v}^{\mathrm{ac}}_{\mathrm{f}} - \boldsymbol{v}^{\mathrm{ac}}_{\mathrm{c}})\right)^{*}\right\}, \tag{7}$$

with

$$\boldsymbol{p}^{\mathrm{g}}_{\min} \le \boldsymbol{p}^{\mathrm{g}} \le \boldsymbol{p}^{\mathrm{g}}_{\max}, \tag{8}$$

$$\boldsymbol{v}^{\mathrm{ac}}_{\mathrm{f}_{\min}} \le |\boldsymbol{v}^{\mathrm{ac}}_{\mathrm{f}}| \le \boldsymbol{v}^{\mathrm{ac}}_{\mathrm{f}_{\max}}, \tag{9}$$

enforcing generator/load power and voltage limits.

D. DC Grid Constraints

Nodal power balance equations of the DC grid can be formulated as

$$\vec{\boldsymbol{L}}^{\top}\vec{\boldsymbol{f}} + \overleftarrow{\boldsymbol{L}}^{\top}\overleftarrow{\boldsymbol{f}} = \boldsymbol{p}^{\mathrm{dc}}, \tag{10}$$

where $\vec{\boldsymbol{f}}$ and $\overleftarrow{\boldsymbol{f}}$ are dictated by nodal DC voltages and the status of transmission lines:

$$\vec{\boldsymbol{f}} = [\vec{\boldsymbol{x}}]\,\mathrm{diag}\{\vec{\boldsymbol{L}}\boldsymbol{v}^{\mathrm{dc}}\boldsymbol{v}^{\mathrm{dc}^{\top}}\vec{\boldsymbol{Y}}^{\top}\} \le \vec{\boldsymbol{f}}_{\max}, \tag{11a}$$

$$\overleftarrow{\boldsymbol{f}} = [\vec{\boldsymbol{x}}]\,\mathrm{diag}\{\overleftarrow{\boldsymbol{L}}\boldsymbol{v}^{\mathrm{dc}}\boldsymbol{v}^{\mathrm{dc}^{\top}}\overleftarrow{\boldsymbol{Y}}^{\top}\} \le \vec{\boldsymbol{f}}_{\max}, \tag{11b}$$

and constrained by thermal limits of the line. Additionally, nodal voltages and power injections of the DC grid should be bounded as follows:

$$\boldsymbol{v}^{\mathrm{dc}}_{\min} \le |\boldsymbol{v}^{\mathrm{dc}}| \le \boldsymbol{v}^{\mathrm{dc}}_{\max}, \tag{12}$$

$$\boldsymbol{p}^{\mathrm{dc}}_{\min} \le \boldsymbol{p}^{\mathrm{dc}} \le \boldsymbol{p}^{\mathrm{dc}}_{\max}. \tag{13}$$

Constraints (12)–(13) enforce steady-state safety requirements. However, due to transient effects, voltage limits in (12) need to be further restricted based on variations in load and generation, as well as the computational time delays in between droop set-point updates. In the following subsection, we formulate complementary voltage constraints that can further improve operational safety.

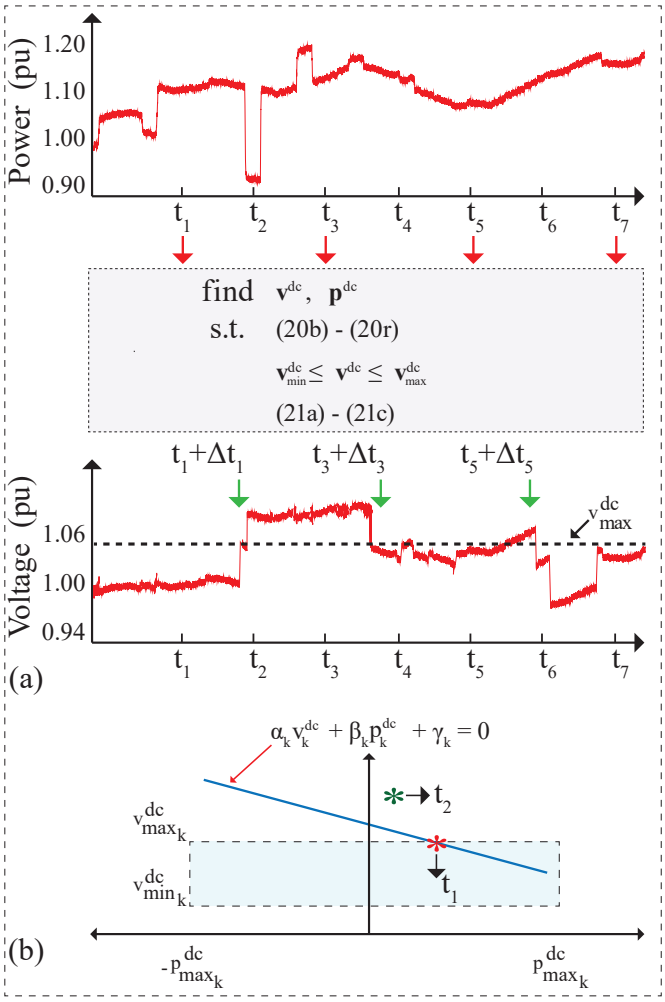

Fig. 2. Droop parameters optimized for the load/generation profile at time t_1 violates the safe operating region until the subsequent update that happens at time $t_3 + \Delta t_3$. (a) Load/generation profile and DC side voltage variation. (b) Generalized voltage-droop characteristics.

E. MTDC Control Strategy

The generalized VSC voltage-droop characteristic can be written as

$$\alpha_k v^{\mathrm{dc}}_k + \beta_k p^{\mathrm{dc}}_k + \gamma_k = 0, \qquad \forall k \in \mathcal{N}, \tag{14}$$

where v^{dc}_k and p^{dc}_k are the DC voltage and power set-points of the VSC at bus k. α_k, β_k, and γ_k are the voltage-droop coefficients of the corresponding converter. In this paper, we assume that $\alpha_k = 1$. Herein, the slope of voltage-droop characteristics is

$$\kappa_k \triangleq \beta_k = \frac{v^{\mathrm{dc}}_{\max_k} - v^{\mathrm{dc}}_{\min_k}}{p^{\mathrm{dc}}_{\max_k} - p^{\mathrm{dc}}_{\min_k}}, \tag{15}$$

and additionally, $\gamma_k = -v^{\mathrm{dc}}_k - \kappa_k p^{\mathrm{dc}}_k$.

Equation (14) guarantees the optimal operation as long as updating droop set-points is fast enough compared to power fluctuations [30]. However, due to the limits in computational speed, this assumption remains valid only if changes in load-/generation are negligible. The unwanted voltage deviation,

caused by rapid changes, can be formulated as

$$\Delta v_k = \kappa_k \Delta p_k, \tag{16}$$

where $\Delta v_k = |v_k^{\mathrm{dc}}(t_1) - v_k^{\mathrm{dc}}(t_2)|$ and $\Delta p_k = |p_k^{\mathrm{dc}}(t_1) - p_k^{\mathrm{dc}}(t_2)|$. We seek to obtain conservative bounds on changes in DC voltage magnitudes, with the aim of ensuring smooth transition to the next operating point.

An illustrative example is provided in Figure 2 to highlight the necessity of this constraint. In Figure 2 (a), the optimizer collects the load profile at time t_1. Optimizing droop set-points requires a computational time, Δt_1. During this time, a noticeable variation in load/generation, as it happens at time t_2, invalidates obtained droop set-points until the subsequent update (at time $t_3 + \Delta t_3$). Thus, droop set-points found at time $t_1 + \Delta t_1$ become harmful for grid operation, particularly within the interval $[t_2, t_3 + \Delta t_3]$.

To prevent this issue, one can underpin droop control with additional constraints so that the DC voltage remains within the pre-described boundaries. We offer the following additional voltage constraints, instead of (12), to guarantee a safe operation under limited load/generation volatility:

$$v_{k_{\min}}^{\mathrm{dc}} + \Delta v_k = v_{k_{\min}}^{\mathrm{dc}} + \kappa_k \Delta p_k \leq v_k^{\mathrm{dc}}, \tag{17}$$

$$v_{k_{\max}}^{\mathrm{dc}} - \Delta v_k = v_{k_{\max}}^{\mathrm{dc}} - \kappa_k \Delta p_k \geq v_k^{\mathrm{dc}}, \tag{18}$$

where Δp_k denotes the power variation in the DC side. A safe operating region can be devised such that corresponding voltage constraints allow power variation up to a specified level. This level can be decided based on the predefined percentage of an existing power injection, i.e., $\Delta p_k \leq \mu_k p_k^{\mathrm{dc}}$.

IV. Topology-cognizant OPF

A. Formulation of the Optimal Grid Topology

In Section III, we have modeled the operational and physical characteristics of a VSC-based MTDC grid. Herein, we devise an objective function that minimizes the total active power loss. The topology-cognizant OPF, with the objective of minimizing total loss, can be formulated as

$$\text{minimize} \quad \mathbf{1}_{|\mathcal{N}|}^{\top}\left(\boldsymbol{G}^{\top}\boldsymbol{p}^{\mathrm{g}} - \boldsymbol{D}^{\top}\boldsymbol{p}^{\mathrm{d}}\right) \tag{19a}$$

$$\text{subject to} \quad \mathrm{real}\{\boldsymbol{s}^{\mathrm{ac}}\} + \boldsymbol{p}^{\mathrm{dc}} + \boldsymbol{a} + [\boldsymbol{b}]|\boldsymbol{i}^{\mathrm{ac}}| + [\boldsymbol{c}]|\boldsymbol{i}^{\mathrm{ac}}|^2 = \mathbf{0} \tag{19b}$$

$$|\boldsymbol{v}_{\mathrm{c}}^{\mathrm{ac}}| \leq \sqrt{\frac{3}{2}}\boldsymbol{v}^{\mathrm{dc}} \tag{19c}$$

$$\boldsymbol{s}^{\mathrm{ac}} = [\boldsymbol{v}_{\mathrm{c}}^{\mathrm{ac}}]\left([\boldsymbol{z}]^{-1}(\boldsymbol{v}_{\mathrm{c}}^{\mathrm{ac}} - \boldsymbol{v}_{\mathrm{f}}^{\mathrm{ac}})\right)^{*} \tag{19d}$$

$$\boldsymbol{p}_{\min}^{\mathrm{ac}} \leq \mathrm{real}\{\boldsymbol{s}^{\mathrm{ac}}\} \leq \boldsymbol{p}_{\max}^{\mathrm{ac}} \tag{19e}$$

$$\boldsymbol{q}_{\min}^{\mathrm{ac}} \leq \mathrm{imag}\{\boldsymbol{s}^{\mathrm{ac}}\} \leq \boldsymbol{q}_{\max}^{\mathrm{ac}} - [\bar{\boldsymbol{q}}^{\mathrm{ac}}]|\boldsymbol{v}_{\mathrm{f}}^{\mathrm{ac}}| \tag{19f}$$

$$\boldsymbol{i}^{\mathrm{ac}} = [\boldsymbol{z}]^{-1}(\boldsymbol{v}_{\mathrm{c}}^{\mathrm{ac}} - \boldsymbol{v}_{\mathrm{f}}^{\mathrm{ac}}) \tag{19g}$$

$$|\boldsymbol{i}^{\mathrm{ac}}| \leq \boldsymbol{i}_{\max}^{\mathrm{ac}} \tag{19h}$$

$$\boldsymbol{G}^{\top}\boldsymbol{p}^{\mathrm{g}} - \boldsymbol{D}^{\top}\boldsymbol{p}^{\mathrm{d}} = \mathrm{real}\left\{[\boldsymbol{v}_{\mathrm{f}}^{\mathrm{ac}}]\left([\boldsymbol{z}]^{-1}(\boldsymbol{v}_{\mathrm{f}}^{\mathrm{ac}} - \boldsymbol{v}_{\mathrm{c}}^{\mathrm{ac}})\right)^{*}\right\} \tag{19i}$$

$$\boldsymbol{p}_{\min}^{\mathrm{g}} \leq \boldsymbol{p}^{\mathrm{g}} \leq \boldsymbol{p}_{\max}^{\mathrm{g}} \tag{19j}$$

$$\boldsymbol{v}_{\mathrm{f}_{\min}}^{\mathrm{ac}} \leq |\boldsymbol{v}_{\mathrm{f}}^{\mathrm{ac}}| \leq \boldsymbol{v}_{\mathrm{f}_{\max}}^{\mathrm{ac}} \tag{19k}$$

$$\boldsymbol{p}^{\mathrm{dc}} = \vec{\boldsymbol{L}}^{\top}\vec{\boldsymbol{f}} + \overleftarrow{\boldsymbol{L}}^{\top}\overleftarrow{\boldsymbol{f}} \tag{19l}$$

$$\boldsymbol{p}_{\min}^{\mathrm{dc}} \leq \boldsymbol{p}^{\mathrm{dc}} \leq \boldsymbol{p}_{\max}^{\mathrm{dc}} \tag{19m}$$

$$|\vec{\boldsymbol{f}} - \mathrm{diag}\{\vec{\boldsymbol{L}}\,\boldsymbol{v}^{\mathrm{dc}}\boldsymbol{v}^{\mathrm{dc}^{\top}}\vec{\boldsymbol{Y}}^{\top}\}| \leq M(1-\vec{\boldsymbol{x}}) \tag{19n}$$

$$|\overleftarrow{\boldsymbol{f}} - \mathrm{diag}\{\overleftarrow{\boldsymbol{L}}\,\boldsymbol{v}^{\mathrm{dc}}\boldsymbol{v}^{\mathrm{dc}^{\top}}\overleftarrow{\boldsymbol{Y}}^{\top}\}| \leq M(1-\vec{\boldsymbol{x}}) \tag{19o}$$

$$|\vec{\boldsymbol{f}}| \leq [\vec{\boldsymbol{f}}_{\max}]\,\vec{\boldsymbol{x}} \tag{19p}$$

$$|\overleftarrow{\boldsymbol{f}}| \leq [\overleftarrow{\boldsymbol{f}}_{\max}]\,\vec{\boldsymbol{x}} \tag{19q}$$

$$\vec{\boldsymbol{x}}_{\min} \leq \vec{\boldsymbol{x}} \leq \vec{\boldsymbol{x}}_{\max} \tag{19r}$$

$$\boldsymbol{v}_{\min}^{\mathrm{dc}} + [\boldsymbol{\kappa}][\boldsymbol{\mu}]\boldsymbol{p}^{\mathrm{dc}} \leq \boldsymbol{v}^{\mathrm{dc}} \leq \boldsymbol{v}_{\max}^{\mathrm{dc}} - [\boldsymbol{\kappa}][\boldsymbol{\mu}]\boldsymbol{p}^{\mathrm{dc}} \tag{19s}$$

$$\text{variables} \quad \boldsymbol{v}^{\mathrm{dc}}, \boldsymbol{p}^{\mathrm{dc}} \in \mathbb{R}^{|\mathcal{N}|}; \quad \boldsymbol{v}_{\mathrm{c}}^{\mathrm{ac}}, \boldsymbol{v}_{\mathrm{f}}^{\mathrm{ac}}, \boldsymbol{i}^{\mathrm{ac}}, \boldsymbol{s}^{\mathrm{ac}} \in \mathbb{C}^{|\mathcal{N}|}$$
$$\boldsymbol{p}^{\mathrm{g}} \in \mathbb{R}^{|\mathcal{G}|} \quad ; \quad \vec{\boldsymbol{f}}, \overleftarrow{\boldsymbol{f}} \in \mathbb{R}^{|\mathcal{L}|}; \quad \vec{\boldsymbol{x}} \in \{0,1\}^{|\mathcal{L}|}$$

where vectors $\boldsymbol{q}_{\min}^{\mathrm{ac}}$, $\boldsymbol{q}_{\max}^{\mathrm{ac}}$, and $\bar{\boldsymbol{q}}^{\mathrm{ac}}$ are set such that (19f) concludes (5). The topology-cognizant OPF formulation (19) suffers from (i) non-convex power flow equations (19d), (19n) and (19o), (ii) non-convex converter loss equations (19b), and (iii) the presence of binary variables, (19r), accounting for the lines' statuses. The non-convex power flow equations corresponding to binary variables in (11a) and (11b) are relaxed using disjunctive inequalities, big-M reformulation, to (19n) and (19o), respectively. Thus, binary variables are defined for each alternative scenario, as the binary variable is either zero or one. Nonlinear components, namely, $\boldsymbol{v}^{\mathrm{dc}}\boldsymbol{v}^{\mathrm{dc}^{\top}}$, $|\boldsymbol{v}_{\mathrm{f}}^{\mathrm{ac}}|$, $|\boldsymbol{v}_{\mathrm{f}}^{\mathrm{ac}}|^2$, $|\boldsymbol{v}_{\mathrm{c}}^{\mathrm{ac}}|^2$, $\mathrm{diag}\{\boldsymbol{v}_{\mathrm{c}}^{\mathrm{ac}}\boldsymbol{v}_{\mathrm{f}}^{\mathrm{ac}^{*}}\}$ and $|\boldsymbol{i}^{\mathrm{ac}}|$ can be convexified via conic inequalities.

B. Convexification of the Problem Formulation

First, we introduce auxiliary variables $\boldsymbol{W}^{\mathrm{dc}} \in \mathbb{S}_{|\mathcal{N}|}$, $\boldsymbol{\phi}^{\mathrm{ac}}, \boldsymbol{t}^{\mathrm{ac}}, \boldsymbol{w}_{\mathrm{cc}}^{\mathrm{ac}}, \boldsymbol{w}_{\mathrm{ff}}^{\mathrm{ac}} \in \mathbb{R}^{|\mathcal{N}|}$, and $\boldsymbol{w}_{\mathrm{cf}}^{\mathrm{ac}} \in \mathbb{C}^{|\mathcal{N}|}$ for nonlinear terms $\boldsymbol{v}^{\mathrm{dc}}\boldsymbol{v}^{\mathrm{dc}^{\top}}$, $|\boldsymbol{i}^{\mathrm{ac}}|$, $|\boldsymbol{i}^{\mathrm{ac}}|^2$, $|\boldsymbol{v}_{\mathrm{c}}^{\mathrm{ac}}|^2$, $|\boldsymbol{v}_{\mathrm{f}}^{\mathrm{ac}}|^2$, and $\mathrm{diag}\{\boldsymbol{v}_{\mathrm{c}}^{\mathrm{ac}}\boldsymbol{v}_{\mathrm{f}}^{\mathrm{ac}^{*}}\}$, respectively. The lifted problem can be formulated as

$$\text{minimize} \quad \mathbf{1}_{|\mathcal{N}|}^{\top}\left(\boldsymbol{G}^{\top}\boldsymbol{p}^{\mathrm{g}} - \boldsymbol{D}^{\top}\boldsymbol{p}^{\mathrm{d}}\right) \tag{20a}$$

$$\text{subject to} \quad \mathrm{real}\{\boldsymbol{s}^{\mathrm{ac}}\} + \boldsymbol{p}^{\mathrm{dc}} + \boldsymbol{a} + [\boldsymbol{b}]\boldsymbol{\phi}^{\mathrm{ac}} + [\boldsymbol{c}]\boldsymbol{t}^{\mathrm{ac}} = \mathbf{0} \tag{20b}$$

$$0 \leq \boldsymbol{w}_{\mathrm{cc}}^{\mathrm{ac}} \leq \frac{3}{2}\mathrm{diag}\{\boldsymbol{W}^{\mathrm{dc}}\} \tag{20c}$$

$$\boldsymbol{s}^{\mathrm{ac}} = \left([\boldsymbol{z}]^{-1}\right)^{*}(\boldsymbol{w}_{\mathrm{cc}}^{\mathrm{ac}} - \boldsymbol{w}_{\mathrm{cf}}^{\mathrm{ac}}) \tag{20d}$$

$$\boldsymbol{p}_{\min}^{\mathrm{ac}} \leq \mathrm{real}\{\boldsymbol{s}^{\mathrm{ac}}\} \leq \boldsymbol{p}_{\max}^{\mathrm{ac}} \tag{20e}$$

$$\boldsymbol{q}_{\min}^{\mathrm{ac}} \leq \mathrm{imag}\{\boldsymbol{s}^{\mathrm{ac}}\} \leq \boldsymbol{q}_{\max}^{\mathrm{ac}} - [\bar{\boldsymbol{q}}^{\mathrm{ac}}]|\boldsymbol{v}_{\mathrm{f}}^{\mathrm{ac}}| \tag{20f}$$

$$\boldsymbol{t}^{\mathrm{ac}} = [|\boldsymbol{z}|]^{-2}(\boldsymbol{w}_{\mathrm{cc}}^{\mathrm{ac}} + \boldsymbol{w}_{\mathrm{ff}}^{\mathrm{ac}} - 2\mathrm{real}\{\boldsymbol{w}_{\mathrm{cf}}^{\mathrm{ac}}\}) \tag{20g}$$

$$\boldsymbol{t}^{\mathrm{ac}} \leq (\boldsymbol{i}_{\max}^{\mathrm{ac}})^2 \tag{20h}$$

$$\boldsymbol{G}^{\top}\boldsymbol{p}^{\mathrm{g}} - \boldsymbol{D}^{\top}\boldsymbol{p}^{\mathrm{d}} = \mathrm{real}\left\{[\boldsymbol{z}]^{-1}(\boldsymbol{w}_{\mathrm{ff}}^{\mathrm{ac}} - \boldsymbol{w}_{\mathrm{cf}}^{\mathrm{ac}})^{*}\right\} \tag{20i}$$

$$\boldsymbol{p}_{\min}^{\mathrm{g}} \leq \boldsymbol{p}^{\mathrm{g}} \leq \boldsymbol{p}_{\max}^{\mathrm{g}} \tag{20j}$$

$$(\boldsymbol{v}_{\mathrm{f}_{\min}}^{\mathrm{ac}})^2 \leq \boldsymbol{w}_{\mathrm{ff}}^{\mathrm{ac}} \leq (\boldsymbol{v}_{\mathrm{f}_{\max}}^{\mathrm{ac}})^2 \tag{20k}$$

$$\boldsymbol{p}^{\mathrm{dc}} = \vec{\boldsymbol{L}}^{\top}\vec{\boldsymbol{f}} + \overleftarrow{\boldsymbol{L}}^{\top}\overleftarrow{\boldsymbol{f}} \tag{20l}$$

$$\boldsymbol{p}_{\min}^{\mathrm{dc}} \leq \boldsymbol{p}^{\mathrm{dc}} \leq \boldsymbol{p}_{\max}^{\mathrm{dc}} \tag{20m}$$

$$|\vec{\boldsymbol{f}} - \mathrm{diag}\{\vec{\boldsymbol{L}}\,\boldsymbol{W}^{\mathrm{dc}}\vec{\boldsymbol{Y}}^{\top}\}| \leq M(1-\vec{\boldsymbol{x}}) \tag{20n}$$

$$|\overleftarrow{\boldsymbol{f}} - \mathrm{diag}\{\overleftarrow{\boldsymbol{L}}\,\boldsymbol{W}^{\mathrm{dc}}\overleftarrow{\boldsymbol{Y}}^{\top}\}| \leq M(1-\vec{\boldsymbol{x}}) \tag{20o}$$

$$|\vec{\boldsymbol{f}}| \le [\vec{\boldsymbol{f}}_{\max}]\,\vec{\boldsymbol{x}} \tag{20p}$$
$$|\overleftarrow{\boldsymbol{f}}| \le [\vec{\boldsymbol{f}}_{\max}]\,\vec{\boldsymbol{x}} \tag{20q}$$
$$\vec{\boldsymbol{x}}_{\min} \le \vec{\boldsymbol{x}} \le \vec{\boldsymbol{x}}_{\max} \tag{20r}$$

$$\boldsymbol{v}^{\mathrm{dc}}_{\min} + [\boldsymbol{\kappa}][\boldsymbol{\mu}]\boldsymbol{p}^{\mathrm{dc}} \ \le \boldsymbol{v}^{\mathrm{dc}} \le \ \boldsymbol{v}^{\mathrm{dc}}_{\max} - [\boldsymbol{\kappa}][\boldsymbol{\mu}]\boldsymbol{p}^{\mathrm{dc}} \tag{20s}$$

$$\sqrt{\boldsymbol{t}^{\mathrm{ac}}} = \boldsymbol{\phi}^{\mathrm{ac}} = |\boldsymbol{i}^{\mathrm{ac}}| \tag{20t}$$

$$\begin{aligned}
&\sqrt{[\vec{\boldsymbol{L}}\mathrm{diag}\{\boldsymbol{W}^{\mathrm{dc}}\}]\ \overleftarrow{\boldsymbol{L}}\mathrm{diag}\{\boldsymbol{W}^{\mathrm{dc}}\}} = \mathrm{diag}\{\vec{\boldsymbol{L}}\boldsymbol{W}^{\mathrm{dc}}\overleftarrow{\boldsymbol{L}}^{\top}\}\\
&\mathrm{diag}\{(\vec{\boldsymbol{L}}-\overleftarrow{\boldsymbol{L}})\boldsymbol{W}^{\mathrm{dc}}(\vec{\boldsymbol{L}}-\overleftarrow{\boldsymbol{L}})^{\top}\} = \big(\vec{\boldsymbol{L}}\boldsymbol{v}^{\mathrm{dc}} - \overleftarrow{\boldsymbol{L}}\boldsymbol{v}^{\mathrm{dc}}\big)^2\\
&\mathrm{diag}\{(\vec{\boldsymbol{L}}+\overleftarrow{\boldsymbol{L}})\boldsymbol{W}^{\mathrm{dc}}(\vec{\boldsymbol{L}}+\overleftarrow{\boldsymbol{L}})^{\top}\} = \big(\vec{\boldsymbol{L}}\boldsymbol{v}^{\mathrm{dc}} + \overleftarrow{\boldsymbol{L}}\boldsymbol{v}^{\mathrm{dc}}\big)^2\\
&\mathrm{diag}\{\boldsymbol{W}^{\mathrm{dc}}\} = \big(\boldsymbol{v}^{\mathrm{dc}}\big)^2
\end{aligned} \tag{20u}$$

$$\begin{aligned}
&\sqrt{[\boldsymbol{w}^{\mathrm{ac}}_{\mathrm{ff}}]\boldsymbol{w}^{\mathrm{ac}}_{\mathrm{cc}}} = |\boldsymbol{w}^{\mathrm{ac}}_{\mathrm{cf}}|,\\
&\boldsymbol{w}^{\mathrm{ac}}_{\mathrm{ff}} + \boldsymbol{w}^{\mathrm{ac}}_{\mathrm{cc}} - 2\,\mathrm{real}\{\boldsymbol{w}^{\mathrm{ac}}_{\mathrm{cf}}\} \ = |\boldsymbol{v}^{\mathrm{ac}}_{\mathrm{c}} - \boldsymbol{v}^{\mathrm{ac}}_{\mathrm{f}}|^2,\\
&\boldsymbol{w}^{\mathrm{ac}}_{\mathrm{ff}} + \boldsymbol{w}^{\mathrm{ac}}_{\mathrm{cc}} + 2\,\mathrm{real}\{\boldsymbol{w}^{\mathrm{ac}}_{\mathrm{cf}}\} \ = |\boldsymbol{v}^{\mathrm{ac}}_{\mathrm{c}} + \boldsymbol{v}^{\mathrm{ac}}_{\mathrm{f}}|^2,\\
&\boldsymbol{w}^{\mathrm{ac}}_{\mathrm{ff}} + \boldsymbol{w}^{\mathrm{ac}}_{\mathrm{cc}} - 2\,\mathrm{imag}\{\boldsymbol{w}^{\mathrm{ac}}_{\mathrm{cf}}\} = |\boldsymbol{v}^{\mathrm{ac}}_{\mathrm{c}} + i\boldsymbol{v}^{\mathrm{ac}}_{\mathrm{f}}|^2,\\
&\boldsymbol{w}^{\mathrm{ac}}_{\mathrm{ff}} + \boldsymbol{w}^{\mathrm{ac}}_{\mathrm{cc}} + 2\,\mathrm{imag}\{\boldsymbol{w}^{\mathrm{ac}}_{\mathrm{cf}}\} = |\boldsymbol{v}^{\mathrm{ac}}_{\mathrm{c}} - i\boldsymbol{v}^{\mathrm{ac}}_{\mathrm{f}}|^2,\\
&\boldsymbol{w}^{\mathrm{ac}}_{\mathrm{ff}} = |\boldsymbol{v}^{\mathrm{ac}}_{\mathrm{f}}|^2, \qquad \boldsymbol{w}^{\mathrm{ac}}_{\mathrm{cc}} = |\boldsymbol{v}^{\mathrm{ac}}_{\mathrm{c}}|^2,
\end{aligned} \tag{20v}$$

variables $\boldsymbol{v}^{\mathrm{ac}}_{\mathrm{c}}, \boldsymbol{v}^{\mathrm{ac}}_{\mathrm{f}}, \boldsymbol{w}^{\mathrm{ac}}_{\mathrm{cc}}, \boldsymbol{w}^{\mathrm{ac}}_{\mathrm{ff}}, \boldsymbol{w}^{\mathrm{ac}}_{\mathrm{cf}}, \boldsymbol{s}^{\mathrm{ac}}, \boldsymbol{i}^{\mathrm{ac}} \in \mathbb{C}^{|\mathcal{N}|}$;
$\boldsymbol{W}^{\mathrm{dc}} \in \mathbb{S}_{|\mathcal{N}|}$; $\boldsymbol{\phi}^{\mathrm{ac}}, \boldsymbol{t}^{\mathrm{ac}}, \boldsymbol{p}^{\mathrm{dc}} \in \mathbb{R}^{|\mathcal{N}|}$; $\boldsymbol{p}^{\mathrm{g}} \in \mathbb{R}^{|\mathcal{G}|}$;
$\vec{\boldsymbol{f}}, \overleftarrow{\boldsymbol{f}} \in \mathbb{R}^{|\mathcal{L}|}$; $\vec{\boldsymbol{x}} \in \{0,1\}^{|\mathcal{L}|}$

The non-convexity of (19) is circumvented by lifting its nonlinear terms into the form of (20) while preserving the equivalency between the two formulations, with the help of additional constraints (20t)-(20v). The main purpose behind this formulation is that it can be immediately convexified via transformation of equalities in (20t)-(20v) to inequalities.

C. SOCP Relaxation

Motivated by [31], a MISOCP formulation can be readily obtained, by relaxing (20t)-(20v) into the following conic and parabolic inequalities:

$$\sqrt{\boldsymbol{t}^{\mathrm{ac}}} \ge \boldsymbol{\phi}^{\mathrm{ac}} \ge |\boldsymbol{i}^{\mathrm{ac}}| \tag{21a}$$

$$\begin{aligned}
&\sqrt{[\vec{\boldsymbol{L}}\mathrm{diag}\{\boldsymbol{W}^{\mathrm{dc}}\}]\ \overleftarrow{\boldsymbol{L}}\mathrm{diag}\{\boldsymbol{W}^{\mathrm{dc}}\}} \ge \mathrm{diag}\{\vec{\boldsymbol{L}}\boldsymbol{W}^{\mathrm{dc}}\overleftarrow{\boldsymbol{L}}^{\top}\}\\
&\mathrm{diag}\{(\vec{\boldsymbol{L}}-\overleftarrow{\boldsymbol{L}})\boldsymbol{W}^{\mathrm{dc}}(\vec{\boldsymbol{L}}-\overleftarrow{\boldsymbol{L}})^{\top}\} \ge (\vec{\boldsymbol{L}}\boldsymbol{v}^{\mathrm{dc}} - \overleftarrow{\boldsymbol{L}}\boldsymbol{v}^{\mathrm{dc}})^2\\
&\mathrm{diag}\{(\vec{\boldsymbol{L}}+\overleftarrow{\boldsymbol{L}})\boldsymbol{W}^{\mathrm{dc}}(\vec{\boldsymbol{L}}+\overleftarrow{\boldsymbol{L}})^{\top}\} \ge (\vec{\boldsymbol{L}}\boldsymbol{v}^{\mathrm{dc}} + \overleftarrow{\boldsymbol{L}}\boldsymbol{v}^{\mathrm{dc}})^2\\
&\mathrm{diag}\{\boldsymbol{W}^{\mathrm{dc}}\} \ge (\boldsymbol{v}^{\mathrm{dc}})^2
\end{aligned} \tag{21b}$$

$$\begin{aligned}
&\sqrt{[\boldsymbol{w}^{\mathrm{ac}}_{\mathrm{ff}}]\boldsymbol{w}^{\mathrm{ac}}_{\mathrm{cc}}} \ge |\boldsymbol{w}^{\mathrm{ac}}_{\mathrm{cf}}|,\\
&\boldsymbol{w}^{\mathrm{ac}}_{\mathrm{ff}} + \boldsymbol{w}^{\mathrm{ac}}_{\mathrm{cc}} - 2\,\mathrm{real}\{\boldsymbol{w}^{\mathrm{ac}}_{\mathrm{cf}}\} \ \ge |\boldsymbol{v}^{\mathrm{ac}}_{\mathrm{c}} - \boldsymbol{v}^{\mathrm{ac}}_{\mathrm{f}}|^2,\\
&\boldsymbol{w}^{\mathrm{ac}}_{\mathrm{ff}} + \boldsymbol{w}^{\mathrm{ac}}_{\mathrm{cc}} + 2\,\mathrm{real}\{\boldsymbol{w}^{\mathrm{ac}}_{\mathrm{cf}}\} \ \ge |\boldsymbol{v}^{\mathrm{ac}}_{\mathrm{c}} + \boldsymbol{v}^{\mathrm{ac}}_{\mathrm{f}}|^2,\\
&\boldsymbol{w}^{\mathrm{ac}}_{\mathrm{ff}} + \boldsymbol{w}^{\mathrm{ac}}_{\mathrm{cc}} - 2\,\mathrm{imag}\{\boldsymbol{w}^{\mathrm{ac}}_{\mathrm{cf}}\} \ge |\boldsymbol{v}^{\mathrm{ac}}_{\mathrm{c}} + i\boldsymbol{v}^{\mathrm{ac}}_{\mathrm{f}}|^2,\\
&\boldsymbol{w}^{\mathrm{ac}}_{\mathrm{ff}} + \boldsymbol{w}^{\mathrm{ac}}_{\mathrm{cc}} + 2\,\mathrm{imag}\{\boldsymbol{w}^{\mathrm{ac}}_{\mathrm{cf}}\} \ge |\boldsymbol{v}^{\mathrm{ac}}_{\mathrm{c}} - i\boldsymbol{v}^{\mathrm{ac}}_{\mathrm{f}}|^2,\\
&\boldsymbol{w}^{\mathrm{ac}}_{\mathrm{ff}} \ge |\boldsymbol{v}^{\mathrm{ac}}_{\mathrm{f}}|^2, \qquad \boldsymbol{w}^{\mathrm{ac}}_{\mathrm{cc}} \ge |\boldsymbol{v}^{\mathrm{ac}}_{\mathrm{c}}|^2,
\end{aligned} \tag{21c}$$

The resulting MISOCP-relaxed topology-cognizant OPF problem (20) with relaxed constraints (21a)-(21c) is compatible with the state-of-the-art branch-and-bound solvers which enables the search for binary variables.

D. Penalization

The proposed convex relaxation (21a)-(21c) can be inexact and fail to provide feasible points for the original nonconvex formulation. In order to ensure that (20t)-(20v) are satisfied, we incorporate a penalty function of the form

$$\begin{aligned}
&\rho_{\check{\boldsymbol{v}}^{\mathrm{dc}},\check{\boldsymbol{v}}^{\mathrm{ac}}_{\mathrm{c}},\check{\boldsymbol{v}}^{\mathrm{ac}}_{\mathrm{f}},\check{\boldsymbol{i}}^{\mathrm{ac}}}(\boldsymbol{W}^{\mathrm{dc}}, \boldsymbol{v}^{\mathrm{dc}}, \boldsymbol{w}^{\mathrm{ac}}_{\mathrm{cc}}, \boldsymbol{v}^{\mathrm{ac}}_{\mathrm{c}}, \boldsymbol{w}^{\mathrm{ac}}_{\mathrm{ff}}, \boldsymbol{v}^{\mathrm{ac}}_{\mathrm{f}}, \boldsymbol{t}^{\mathrm{ac}}, \boldsymbol{i}^{\mathrm{ac}}) =\\
&\quad \eta^{\mathrm{dc}}\big(\mathrm{tr}\{\boldsymbol{W}^{\mathrm{dc}}\} - 2(\check{\boldsymbol{v}}^{\mathrm{dc}})^{\top}\boldsymbol{v}^{\mathrm{dc}} + \|\check{\boldsymbol{v}}^{\mathrm{dc}}\|_2^2\big) + && \text{(22a)}\\
&\quad \eta^{\mathrm{ac}}_{\mathrm{c}}\big(\mathbf{1}^{\top}_{|\mathcal{N}|}\boldsymbol{w}^{\mathrm{ac}}_{\mathrm{cc}} - (\check{\boldsymbol{v}}^{\mathrm{ac}}_{\mathrm{c}})^*\boldsymbol{v}^{\mathrm{ac}}_{\mathrm{c}} - (\boldsymbol{v}^{\mathrm{ac}}_{\mathrm{c}})^*\check{\boldsymbol{v}}^{\mathrm{ac}}_{\mathrm{c}} + \|\check{\boldsymbol{v}}^{\mathrm{ac}}_{\mathrm{c}}\|_2^2\big) + && \text{(22b)}\\
&\quad \eta^{\mathrm{ac}}_{\mathrm{f}}\big(\mathbf{1}^{\top}_{|\mathcal{N}|}\boldsymbol{w}^{\mathrm{ac}}_{\mathrm{ff}} - (\check{\boldsymbol{v}}^{\mathrm{ac}}_{\mathrm{f}})^*\boldsymbol{v}^{\mathrm{ac}}_{\mathrm{f}} - (\boldsymbol{v}^{\mathrm{ac}}_{\mathrm{f}})^*\check{\boldsymbol{v}}^{\mathrm{ac}}_{\mathrm{f}} + \|\check{\boldsymbol{v}}^{\mathrm{ac}}_{\mathrm{f}}\|_2^2\big) + && \text{(22c)}\\
&\quad \eta^{\mathrm{ac}}_{\mathrm{i}}\big(\mathbf{1}^{\top}_{|\mathcal{N}|}\boldsymbol{t}^{\mathrm{ac}} - (\check{\boldsymbol{i}}^{\mathrm{ac}})^*\boldsymbol{i}^{\mathrm{ac}} - (\boldsymbol{i}^{\mathrm{ac}})^*\check{\boldsymbol{i}}^{\mathrm{ac}} + \|\check{\boldsymbol{i}}^{\mathrm{ac}}\|_2^2\big) && \text{(22d)}
\end{aligned}$$

into the objective of convex relaxation, where $(\check{\boldsymbol{v}}^{\mathrm{dc}}, \check{\boldsymbol{v}}^{\mathrm{ac}}_{\mathrm{c}}, \check{\boldsymbol{v}}^{\mathrm{ac}}_{\mathrm{f}}, \check{\boldsymbol{i}}^{\mathrm{ac}}) \in \mathbb{R}^{|\mathcal{N}|} \times \mathbb{R}^{|\mathcal{C}|} \times \mathbb{R}^{|\mathcal{C}|} \times \mathbb{R}^{|\mathcal{C}|}$ can be any arbitrary initial point. As shown in [22], the proper selection of penalty coefficients $\eta^{\mathrm{dc}}, \eta^{\mathrm{ac}}_{\mathrm{c}}, \eta^{\mathrm{ac}}_{\mathrm{f}}, \eta^{\mathrm{ac}}_{\mathrm{i}} \ge 0$ guarantees the recovery of near-optimal feasible points. In the following section, we show that the simple choice of parameters

$$\check{\boldsymbol{v}}^{\mathrm{dc}} = \check{\boldsymbol{v}}^{\mathrm{ac}}_{\mathrm{c}} = \check{\boldsymbol{v}}^{\mathrm{ac}}_{\mathrm{f}} = \check{\boldsymbol{i}}^{\mathrm{ac}} = 0, \tag{23a}$$
$$\eta^{\mathrm{dc}} = 10^{-4}, \qquad \eta^{\mathrm{ac}}_{\mathrm{i}} = 10^{-5}, \qquad \eta^{\mathrm{ac}}_{\mathrm{c}} = \eta^{\mathrm{ac}}_{\mathrm{f}} = 0, \tag{23b}$$

can reliably solve the original non-convex problem in practice.

V. Case Studies

A. System Setup

The modified CIGRE B4 DC grid benchmark [32], equipped with switches to open/close transmission lines, is shown in Figure 3. This grid is emulated in a HIL environment, with two dSPACE DS1202 MicroLabBoxes to implement droop controllers for individual VSCs, and two Typhoon HIL604 units to emulate VSCs and transmission lines, as shown in Figure 4. The proposed optimization algorithm runs on a 16-core Xeon PC with 256 GB RAM. The TCP/IP link between Typhoon HIL/MATLAB/dSPACE MicroLabBoxes shares the load, set-point information, and the status of switching devices at every five second. Resulting SOCP and MISOCP problems are solved in the CVX v2.1 environment [33] using the conic mixed-integer solver GUROBI v8.0.1 [34]. In the following studies, four time intervals, $[0\mathrm{s}, 120\mathrm{s}]$, $[120\mathrm{s}, 220\mathrm{s}]$, $[220\mathrm{s}, 320\mathrm{s}]$, and $[320\mathrm{s}, 420\mathrm{s}]$, are considered.

The rated power of each VSC is 1200 MW. Variable loads are attached to bus 1 and bus 4. The bounds on power constraints for AC and DC sides are $p^{\mathrm{dc}}_{\min_k} = p^{\mathrm{ac}}_{\min_k} = -1200\,\mathrm{MW}$ and $p^{\mathrm{dc}}_{\min_k} = p^{\mathrm{ac}}_{\max_k} = 1200\,\mathrm{MW}$ for every VSC at bus $k \in \mathcal{N}$. The loss coefficients in (1) are $a_k = 2.65 \times 10^{-5}$, $b_k = 3.7 \times 10^{-5}$, and $c_k = 3.6 \times 10^{-5}$ for every VSC at bus $k \in \mathcal{N}$. The converter constant and nominal apparent power in (5) are $m_b = 0.6$ and $|\bar{\boldsymbol{s}}^{\mathrm{ac}}| = 1.2$ pu, respectively. Phase-reactor parameters in (5) are $r_k = 2.5 \times 10^{-6}$ and $x_k = 4 \times 10^{-4}$ for every $k \in \mathcal{N}$. VSC parameters are

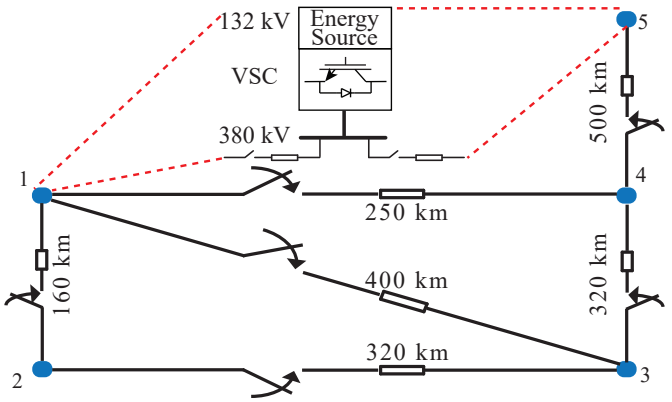

Fig. 3. The modified CIGRE B4 DC grid equipped with line switches. DC cable resistance for +/-400 kv is 0.0095 Ω/km.

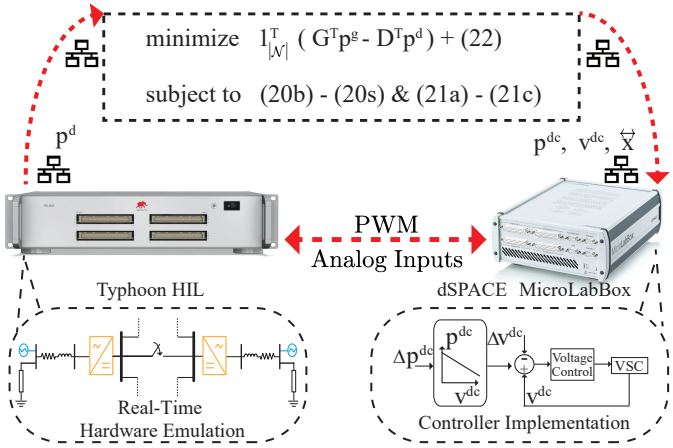

Fig. 4. Topology-cognizant OPF testbed on a HIL system consisting of real-time hardware emulation (Typhoon HIL), controller implementation (dSPACE), and TCP/IP communication link.

$i^{\text{ac}}_{\text{c}_{\max}} = 1.0526$ and $v^{\text{ac}}_{\text{c}_{\max}} = 1.05$. The maximum modulation factor in (2) is $m = 1$. The voltage bounds are 0.94 pu (352.7 kV) and 1.06 pu (402.8 kV). The lines are rated at $\vec{f}_{l_{\max}} = 0.3$ pu (300 MW) for every $l \in \mathcal{L}$. Moreover, the big-M constant in (19) and (20) is $M = 500$. Safety constraint coefficients in (20s) are $\mu_k = 10\%$ and $\kappa_k = 5\%$ for every VSC at bus $k \in \mathcal{N}$. Penalty coefficients in (22) are chosen from (23).

B. MTDC Grid Operation with Static OPF

Static OPF refers to the problem (20) with a connected grid such that $\vec{x}_{l_{\min}} = \vec{x}_{l_{\max}} = 1$ for every $l \in \mathcal{L}$. If OPF results do not update the set-points of the local droop controller, they arrive at a feasible operating condition shown in Figure 5. The main goal of a local droop controller is to ensure stable operation of a VSC in voltage-power tracking and meeting the load demand. Local controllers are not concerned with the optimal operation of the MTDC grid. Hence, the total loss obtained via local controllers can always be reduced by considering the optimality conditions. The total loss obtained via local controllers and the static OPF are given in Table I. Upon enforcing the outcome of the static OPF, roughly around

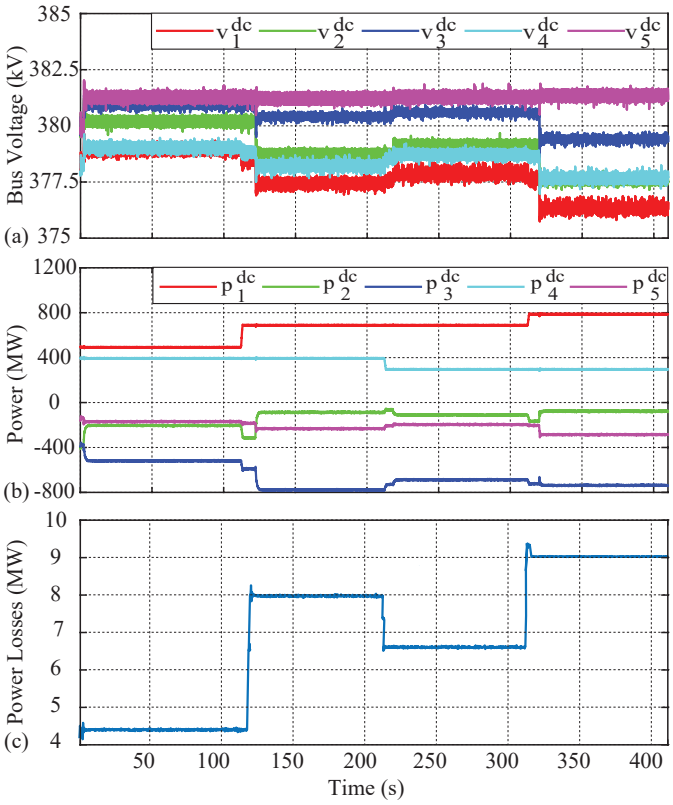

Fig. 5. MTDC operation with droop control under varying load: (a) DC side voltage variation, (b) DC side power variation, and (c) Total power losses.

TABLE I
TOTAL LOSSES WITH DIFFERENT APPROACHES (MW)

Method \ Time interval (s)	0-120	120-220	220-320	320-420
Local droop controller	4.40	8.00	6.50	9.00
Static OPF	3.97	7.16	5.86	8.08
Topology-cognizant OPF without the safety constraints (20) without (20s)	3.78	6.19	5.11	7.11
Topology-cognizant OPF with the safety constraints (20) with (20s)	3.80	6.22	5.14	7.13

10% reduction in loss is reported compared to results obtained via local droop controllers alone. The average computation time to solve the static OPF and update droop set-points is 1.4 s.

C. MTDC Grid Operation with Topology-cognizant OPF

The problem (20), with and without the constraints in (20s), is solved to determine the optimal grid topology with the aim of reducing the total loss. The outcome of topology-cognizant OPF problem without voltage safety limits in (20s) further reduces the total loss by 4.79%, 13.54%, 12.80%, and 12.00% for the four time intervals as compared to the static OPF scenarios. Based on the outcome of (20) (except (20s)),

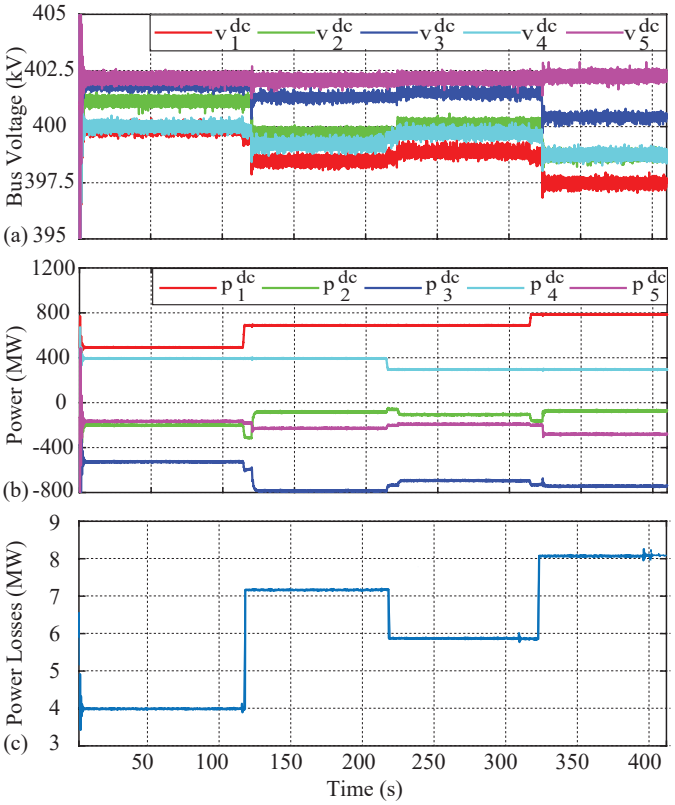

Fig. 6. MTDC operation with static OPF under varying load: (a) DC side voltage variation, (b) DC side power variation, and (c) Total power losses.

$\vec{x}_{2-3}$ is always disconnected, while $\vec{x}_{1-4}$ is disconnected only during $[0\text{s}, 120\text{s}]$ time interval. Eventhough the total loss is further reduced, the voltage safety limits are violated at bus 5 due to load fluctuations and the computation time involved in updating droop set-points, see Figure 7 (a). Additional safety constraints in (20s) mitigate any voltage violation in response to power fluctuations in between two droop set-points updates as shown in Figure 8 (a). This safer operation comes with a slightly higher total loss compared to the case ignoring (20s); Nevertheless, it still offers remarkable reduction in total loss as compared to the static OPF. The total loss obtained by the topology-cognizant OPF with and without the constraints in (20s) are given in Table I. Total losses for different loading profiles are about 0.42%, 0.57%, 0.52%, and 0.65% of the total load demand for the four time intervals. The converter losses obtained from SOCP relaxation approach are about 7.31%, 4.71%, 5.65%, and 4.18% of the total loss in corresponding intervals. Updating droop set-points, that are sent to VSCs every five second, takes around 2.5 s.

VI. Conclusion

This paper offers a convex optimization framework to solve the grid topology-cognizant OPF problem for MTDC grids. It provides local voltage and power set-points for droop controllers of VSCs as well as the operational status of transmission lines. Additional constraints, that sustain safe operation in response to the power fluctuation in between two droop updates, are integrated into the proposed formulation. The

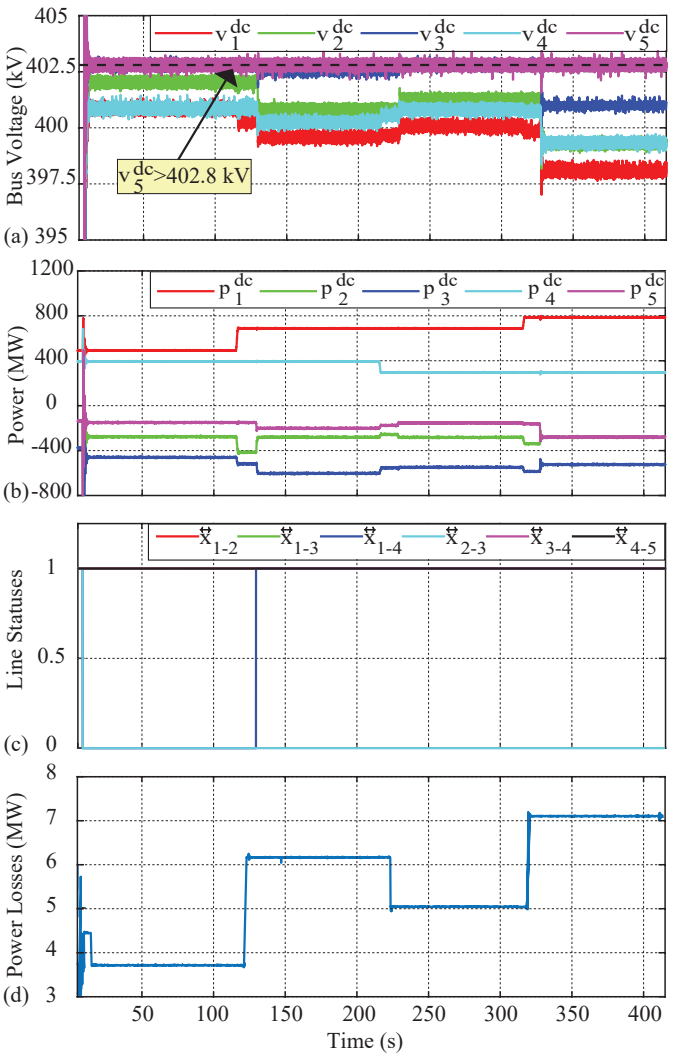

Fig. 7. MTDC operation with topology-cognizant OPF disregarding voltage safety constraints in (20s). The variations in load/generation have DC voltage at bus 5 violate the safety limit: (a) DC side voltage variation (dotted line shows the safety limit, $v^{\text{dc}}_{\max} = 402.8$ kV), (b) DC side power variation, (c) Line statuses, and (d) Total power losses.

resulting MINLP embodies three types of non-convexity due to the quadratic power flow equations, incorporation of switching decisions, and the nonlinear converter loss equations. We relax this problem into a tractable MISOCP that can be solved using standard branch-and-bound solvers. Experimental results verify the efficacy of the proposed method.

References

[1] U. Karaagac, J. Mahseredjian, L. Cai, and H. Saad, "Offshore wind farm modeling accuracy and efficiency in mmc-based multi-terminal hvdc connection," *IEEE Transactions on Power Delivery*, vol. PP, no. 99, pp. 1–1, 2016.

[2] D. Van Hertem and M. Ghandhari, "Multi-terminal vsc hvdc for the european supergrid: Obstacles," *Renewable and sustainable energy reviews*, vol. 14, no. 9, pp. 3156–3163, 2010.

[3] M. K. Bucher, R. Wiget, G. Andersson, and C. M. Franck, "Multiterminal hvdc networks-What is the preferred topology?" *IEEE Transactions on Power Delivery*, vol. 29, no. 1, pp. 406–413, Feb 2014.

[4] Mingxia Zhou, Sheng Li, Jianhua Zhang, Zongqi Liu, and Yinhui Li, "A study on the black start capability of VSC-HVDC using soft-starting mode," in *2009 IEEE 6th International Power Electronics and Motion Control Conference*, May 2009, pp. 910–914.

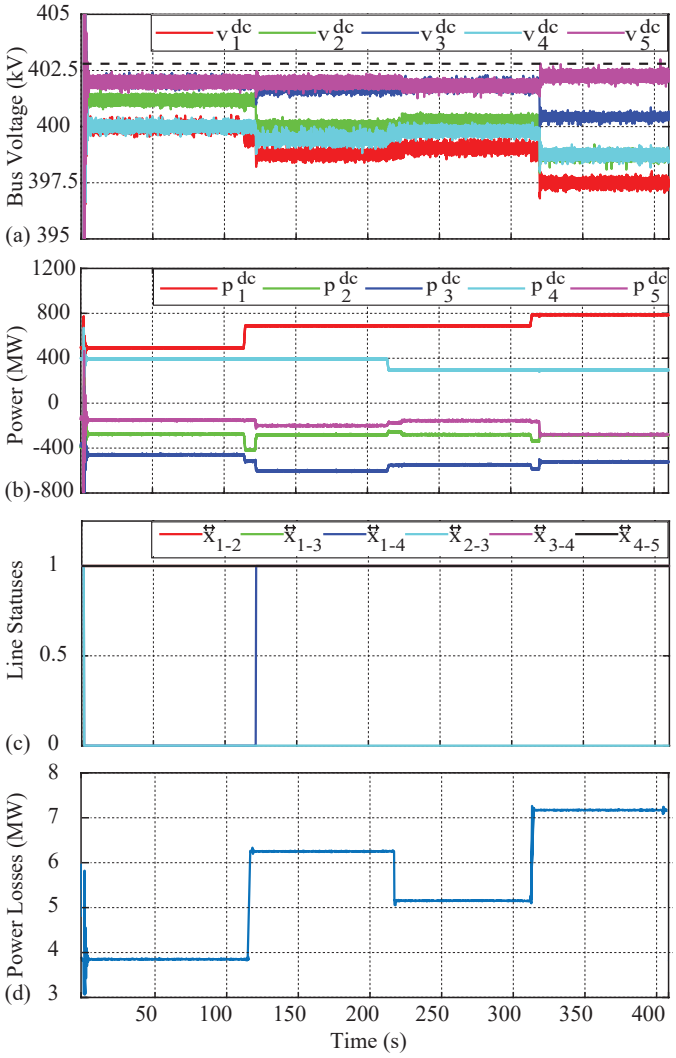

Fig. 8. MTDC operation with topology-cognizant OPF considering the voltage safety constraints in (20s): (a) DC side voltage variation (dotted line shows the safety limit, $v_{\max}^{\mathrm{dc}} = 402.8$ kV), (b) DC side power variation, (c) Line statuses, and (d) Total power losses.

[5] F. Thams, R. Eriksson, and M. Molinas, "Interaction of droop control structures and its inherent effect on the power transfer limits in multi-terminal VSC-HVDC," *IEEE Transactions on Power Delivery*, vol. 32, no. 1, pp. 182–192, Feb 2017.

[6] A. Yazdani and R. Iravani, *Voltage-sourced converters in power systems*. Wiley Online Library, 2010, vol. 34.

[7] N. Yousefpoor, S. Kim, and S. Bhattacharya, "Multi-terminal dc grid control under loss of terminal station," in *2014 IEEE Energy Conversion Congress and Exposition (ECCE)*, Sept 2014, pp. 744–749.

[8] J. Beerten, S. Cole, and R. Belmans, "Modeling of multi-terminal vsc hvdc systems with distributed dc voltage control," *IEEE Transactions on Power Systems*, vol. 29, no. 1, pp. 34–42, Jan 2014.

[9] K. Rouzbehi, A. Miranian, J. I. Candela, A. Luna, and P. Rodriguez, "A generalized voltage droop strategy for control of multiterminal dc grids," *IEEE Transactions on Industry Applications*, vol. 51, no. 1, pp. 607–618, Jan 2015.

[10] C. Gavriluta, J. I. Candela, J. Rocabert, A. Luna, and P. Rodriguez, "Adaptive droop for control of multiterminal dc bus integrating energy storage," *IEEE Transactions on Power Delivery*, vol. 30, no. 1, pp. 16–24, Feb 2015.

[11] C. Gavriluta, I. Candela, A. Luna, A. Gomez-Exposito, and P. Rodriguez, "Hierarchical control of hv-mtdc systems with droop-based primary and opf-based secondary," *IEEE Transactions on Smart Grid*, vol. 6, no. 3, pp. 1502–1510, May 2015.

[12] Q. Nguyen, G. Todeschini, and S. Santoso, "Power flow in a multi-frequency hvac and hvdc system: Formulation, solution, and validation," *IEEE Transactions on Power Systems*, vol. 34, no. 4, pp. 2487–2497, July 2019.

[13] M. A. Abdelwahed and E. F. El-Saadany, "Power sharing control strategy of multiterminal VSC-HVDC transmission systems utilizing adaptive voltage droop," *IEEE Transactions on Sustainable Energy*, vol. 8, no. 2, pp. 605–615, April 2017.

[14] X. Lu, J. M. Guerrero, K. Sun, and J. C. Vasquez, "An improved droop control method for dc microgrids based on low bandwidth communication with dc bus voltage restoration and enhanced current sharing accuracy," *IEEE Transactions on Power Electronics*, vol. 29, no. 4, pp. 1800–1812, April 2014.

[15] T. M. Haileselassie and K. Uhlen, "Impact of dc line voltage drops on power flow of mtdc using droop control," *IEEE Transactions on Power Systems*, vol. 27, no. 3, pp. 1441–1449, Aug 2012.

[16] L. Xiao, Z. Xu, T. An, and Z. Bian, "Improved analytical model for the study of steady state performance of droop-controlled VSC-MTDC systems," *IEEE Transactions on Power Systems*, 2016.

[17] A. Nikoobakht, J. Aghaei, T. Niknam, V. Vahidinasab, H. Farahmand, and M. Korps, "Towards robust opf solution strategy for the future ac/dc grids: case of VSC-HVDC-connected offshore wind farms," *IET Renewable Power Generation*, vol. 12, no. 6, pp. 691–701, 2018.

[18] F. Sun, J. Ma, M. Yu, and W. Wei, "A robust optimal coordinated droop control method for multiple vscs in ac-dc distribution network," *IEEE Transactions on Power Systems*, pp. 1–1, 2019.

[19] B. Li, Q. Li, Y. Wang, W. Wen, B. Li, and L. Xu, "A novel method to determine droop coefficients of dc voltage control for VSC-MTDC system," *IEEE Transactions on Power Delivery*, pp. 1–1, 2020.

[20] W. Feng, L. A. Tuan, L. B. Tjernberg, A. Mannikoff, and A. Bergman, "A new approach for benefit evaluation of multiterminal vschvdc using a proposed mixed ac/dc optimal power flow," *IEEE Transactions on Power Delivery*, vol. 29, no. 1, pp. 432–443, Feb 2014.

[21] S. H. Low, "Convex relaxation of optimal power flow-part i: Formulations and equivalence," *IEEE Transactions on Control of Network Systems*, vol. 1, no. 1, pp. 15–27, March 2014.

[22] R. Madani, S. Sojoudi, and J. Lavaei, "Convex relaxation for optimal power flow problem: Mesh networks," *IEEE Transactions on Power Systems*, vol. 30, no. 1, pp. 199–211, Jan 2015.

[23] B. Kocuk, S. S. Dey, and X. A. Sun, "Strong socp relaxations for the optimal power flow problem," *Operations Research*, vol. 64, no. 6, pp. 1177–1196, 2016.

[24] S. Bahrami, F. Therrien, V. W. S. Wong, and J. Jatskevich, "Semidefinite relaxation of optimal power flow for acdc grids," *IEEE Transactions on Power Systems*, vol. 32, no. 1, pp. 289–304, Jan 2017.

[25] M. Baradar, M. R. Hesamzadeh, and M. Ghandhari, "Second-order cone programming for optimal power flow in VSC-Type ac-dc grids," *IEEE Transactions on Power Systems*, vol. 28, no. 4, pp. 4282–4291, Nov 2013.

[26] K. W. Hedman, S. S. Oren, and R. P. O'Neill, "A review of transmission switching and network topology optimization," in *2011 IEEE Power and Energy Society General Meeting*, July 2011, pp. 1–7.

[27] K. W. Hedman, R. P. O'Neill, E. B. Fisher, and S. S. Oren, "Optimal transmission switchingsensitivity analysis and extensions," *IEEE Transactions on Power Systems*, vol. 23, no. 3, pp. 1469–1479, Aug 2008.

[28] B. Kocuk, S. S. Dey, and X. A. Sun, "New formulation and strong misocp relaxations for ac optimal transmission switching problem," *IEEE Transactions on Power Systems*, vol. 32, no. 6, pp. 4161–4170, Nov 2017.

[29] R. A. Jabr, R. Singh, and B. C. Pal, "Minimum loss network reconfiguration using mixed-integer convex programming," *IEEE Transactions on Power Systems*, vol. 27, no. 2, pp. 1106–1115, May 2012.

[30] E. Prieto-Araujo, A. Egea-Alvarez, S. Fekriasl, and O. Gomis-Bellmunt, "Dc voltage droop control design for multiterminal hvdc systems considering ac and dc grid dynamics," *IEEE Transactions on Power Delivery*, vol. 31, no. 2, pp. 575–585, April 2016.

[31] F. Zohrizadeh, M. Kheirandishfard, E. Q. Jnr, and R. Madani, "Penalized parabolic relaxation for optimal power flow problem," in *2018 IEEE Conference on Decision and Control (CDC)*, Dec 2018, pp. 1616–1623.

[32] T. K. Vrana, Y. Yang, D. Jovcic, S. Dennetière, J. Jardini, and H. Saad, "The cigre b4 dc grid test system," *Electra*, vol. 270, no. 1, pp. 10–19, 2013.

[33] M. Grant and S. Boyd, "CVX: Matlab software for disciplined convex programming, version 2.1," http://cvxr.com/cvx, Mar. 2014.

[34] L. Gurobi Optimization, "Gurobi optimizer reference manual," 2018. [Online]. Available: http://www.gurobi.com